MHD Convection of an Al_2O_3–Cu/Water Hybrid Nanofluid in an Inclined Porous Cavity with Internal Heat Generation/Absorption

Chamkha, Ali Jawad •
Institute of Research and Development, Duy Tan University, Da Nang 550000, VIETNAM

Armaghani, Taher
Department of Engineering, West Tehran Branch, Islamic Azad University, Tehran, IRAN

Mansour, Mohamed Ahmed
Department of Mathematics, Assuit University, Faculty of Science, Assuit, EGYPT

Rashad, Ahmed Mohamed
Department of Mathematics, Aswan University, Faculty of Science, Aswan, 81528, EGYPT

Kargarsharifabad, Hadi* +
Energy and Sustainable Development Research Center, Semnan Branch, Islamic Azad University, Semnan, I.R. IRAN

.**ABSTRACT:** *In Present communication, the transference of the hybrid nanofluids due to the natural propulsive like shrinkage and relaxation of the flexible walls and the motion has serious applications in several embryonic technologies. Stimulated by the multi-disciplinary development and study of this trend, a mathematical model is suggested to explore the numerical simulation of the hybrid nanofluid flow inside a slant porous cavity to determine the impact of volume fraction, Rayleigh number, heat generation and heat source length, and location on magneto-free convective with entropy analysis. The governing nonlinear problem is converted into non-dimensional partial equations via suitably adjusted transformations. The Successive Under-Relaxation (SUR) technique has been incorporated to find solutions to the non-linear problem. Variation in entropy generation and heat transfer characteristics and thermal performance criteria has been noted for various fluid parameters. The results are plotted graphically. The outcomes indicate that the thermal performance reduces more in the case of high volume fraction in comparison with low concentration. The addition of nanoparticles for several Rayleigh numbers causes the thermal performance to be declined.*

KEYWORDS: *Hybrid Nanofluid; Heat generation; Entropy generation; MHD; Thermal performance criteria; Porous medium.*

* *To whom correspondence should be addressed.*
+ *E-mail*: *h.kargar@semnaniau.ac.ir*
• *Other Address: Institute of Theoretical and Applied Research (ITAR), Duy Tan University, Hanoi 100000, VIETNAM*
1021-9986/2022/3/936-956 21/$/7.01

INTRODUCTION

Heat transfer by natural or free convection is a very important industrial problem for its various uses such as solar collectors, cooling electronic devices, and food drying [1]. There are various techniques for heat transfer enhancement titled active and passive methods [2, 3]. Using nanoparticles, porous media, and changing the flow regime in a base fluid are the possible methods for increasing the free convection heat transfer.

Nanotechnology is recently a very hotly debated issue of study. Every day, nanotechnology takes an interest in certifiable problems. It plays a significant role in processes concerned with industry, biomedicine, medicine, and technology. The key importance of nanotechnology is to improve the heat transference mechanism in several electronic devices in order to enhance their performance. A mixture of nanosized particles into a standard fluid like water, ethylene glycol, oil, etc. is called nanofluid. Using of nanofluids as conventional fluids in heat transfer and the study of their effects on it has been investigated in most of the earlier research [4–8]. *Habibi et al*. [9], *Goodarzi et al.* [10] and many other researchers [11–13] investigate the nanofluid for free convection heat transfer in the cavity. Recently,

Hybrid nanofluids constitute a novel diversity of nanoscale liquids in which various sizes and material metallic nanoparticles are embedded in a standard liquid to realize eminent thermal performance. They are an amendment of conventional nonliquids since different nanoparticles are suspended together in the transference liquid either in composite or mixture form [14, 15]. On the other hand, mixing two different nanoparticles in based fluid(s) called hybrid nanofluid [16, 17]. Hybrid nanofluids are increasingly being used in several sections of nanotechnology including smart pumping systems, medicine, coatings, fuels, lubricants, and adhesives. Various analytical and experimental investigations of hybrid nanofluids have been performed in recent years.

A correct combination of nanoparticles and mixing them with base fluid can lead to a hybrid nanofluid with better thermophysical characteristics [18, 19] and an effective impact on heat transfer [20–23]. Numerous studies have been conducted on the effect of hybrid nanofluid on free convection heat transfer [24–26]. *Mehryan et al*. [27] studied the effect of the Al_2O_3-Cu/water hybrid nanofluid on free convection heat transfer in a porous cavity and observed that hybrid nanofluid leads to a reduction in free convective heat transfer.

Porous media is another way of heat transfer enhancement [28, 29]. This phenomenon has been addressed in some studies by partially and fully filling the space with porous medium and the effect of optimum porous layer thickness, porosity ratio and etc. [30–34]. Using nanofluid with a porous media is an efficient way to increase heat transfer performance [35, 36]. *Hatami et al.* [37] investigated the effect of nanofluid heat transfer in a T-shaped porous. Their results indicated that Darcy's number and porosity percentage have a direct relationship in heat transfer. A study of combined convection with CuO/Water nanofluid in a square porous cavity indicated that the cylinder rotational speed and nanofluid volume fraction increased heat transfer [38]. Free convection heat transfer of hybrid nanofluid within a porous medium was studied in [27, 39, 40].

Sometimes the magnetic field affects the flow of electrically conducting fluids [41]. In this situation, the flow and heat convection effect by a body force is named Lorentz force [41–45] and is frequently entitled magnetohydrodynamic (MHD) convection. Interest in understanding MHD convection, especially in enclosure-free convection has increased [46–49].

The use of nanofluid with the porous medium is a possible solution when a magnetic field weakens the convection flow field [50]. This strategy is investigated by *Rashad et al.* [51] and *Ahmed* and *Rashad* [52]. *Sajjadi et al.* [53] simulated MHD free convection of multi-walled carbon nanotube (MWCNT)–Fe_3O_4/water hybrid nanofluid in a porous enclosure and the effect of various parameters have been analyzed. Also, the free convection heat transfer of a hybrid nanofluid within a porous medium under a nonuniform magnetic field has been investigated [54].

For reaching an optimum thermal performance, only the first law of thermodynamics analysis is not sufficient, and studying the second law of thermodynamics analysis is necessary for thermal systems [55–59]. *Aghaei et al.* [60] reported the effect of horizontal and vertical elliptic baffles inside an enclosure on the mixed convection of nanofluid and its entropy generation. *Goodarzi et al.* [61] studied the study of entropy generation due to coupled laminar and turbulent mixed convection and thermal radiation in an enclosure filled with a semitransparent medium. Consideration of entropy generation due to free convection

of nanofluids in porous media has been analyzed in the literature [12, 62, 63]. In addition to examining the effect of those parameters, the effect of magnet has also been investigated [51, 64–66].

Due to the continuous literature survey, we did not find a study that concentrates on the hybrid nanofluid entropy generation in an inclined porous cavity with heat generation and under a magnetic field. Thus, in this investigation, we present the analysis of entropy generation due to internal heat generation and heat transfer of MHD-free convective using a hybrid nanofluid as the working fluid. We deal with this geometry because it is very useful in cooling systems of nuclear and chemical reactors, and electronic components. In our current work, we studied the impacts of MHD and hybrid nanofluid volume fraction on heat transfer and second-law analysis that Ref. [67] didn't investigate.

THEORETICAL SECTION

Problem Description

Fig. 1 exhibits the schematic of a two-dimensional inclined square porous cavity of length (H). The inclination angle (Φ) of the enclosure is from the horizontal in the counterclockwise trend. The magnetic field with a strength B_0 was applied perpendicular to the left side of the enclosure. A part of the bottom and upper wall (with length b) is under the influence of constant heat flux (q") and cooled temperature (Tc), respectively. The rest of the remaining parts of the mentioned two walls and the left and right walls of the enclosure are assumed to be adiabatic. The assumptions of incompressible, laminar, and heat generation at a uniform rate Q_0 are used for modeling the nanofluid. Also, the nanoparticles, base fluid, and porous media are assumed to be in thermal equilibrium conditions. Also, the nanofluid heat transfer is modeled by single-phase approaches. This geometry is very applicable to cooling electronic devices.

Governing equations

Conservation equations of continuity, momentum, and energy were used for governing equations with a single-phase approach. Thermo-physical properties of the liquid phase are assumed constant except for density. The Boussinesq approximation is used for consideration of density variation. The Darcy-Brinkman formulation is applied to describe the flow within the porous layer. According to the above, the governing equations can be written as [28]:

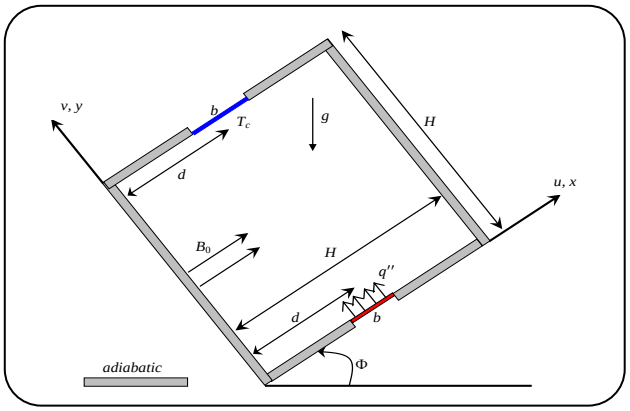

Fig. 1: Schematic diagram of the problem under the consideration.

$$\frac{\partial u}{\partial x}+\frac{\partial v}{\partial y}=0 \tag{1}$$

$$\frac{1}{\varepsilon^2}\left(u\frac{\partial u}{\partial x}+v\frac{\partial u}{\partial y}\right)=-\frac{1}{\rho_{hnf}}\frac{\partial p}{\partial x}+ \tag{2}$$

$$\frac{\nu_{hnf}}{\varepsilon}\nabla^2 u-\frac{\nu_{h_{nf}}}{K}u+\frac{(\rho\beta)_{hnf}}{\rho_{hnf}}g\left(T-T_c\right)\sin\Phi$$

$$\frac{1}{\varepsilon^2}\left(u\frac{\partial v}{\partial x}+v\frac{\partial v}{\partial y}\right)=-\frac{1}{\rho_{hnf}}\frac{\partial p}{\partial y}+ \tag{3}$$

$$\frac{\nu_{hnf}}{\varepsilon}\nabla^2 v-\frac{\nu_{hnf}}{K}v+\frac{(\rho\beta)_{hnf}}{\rho_{hnf}}g\left(T-T_c\right)\cos\Phi-\frac{\sigma_{hnf}B_0^2}{\rho_{hnf}}v$$

$$\frac{1}{\varepsilon}\left(u\frac{\partial T}{\partial x}+v\frac{\partial T}{\partial y}\right)=\alpha_{eff,hnf}\nabla^2 T+ \tag{4}$$

$$\frac{1}{\varepsilon\left(\rho c_p\right)_{hnf}}Q_0\left(T-T_c\right)$$

with the boundary conditions as follows:

$$x=0,\ x=H,\ y=0,\ y=H\Rightarrow u=v=0 \tag{5}$$

$$\left(d-0.5b\right)\le x\le\left(d+0.5b\right)\ \text{and}\ \ y=0\Rightarrow\frac{\partial T}{\partial y}=-\frac{q''}{k_{eff,hnf}}$$

Other remaining parts on the wall

$$y=0\Rightarrow\frac{\partial T}{\partial y}=0,\ \ x=0,\ H\Rightarrow\frac{\partial T}{\partial y}=0$$

$$\left(d-0.5b\right)\le x\le\left(d+0.5b\right)\ \text{and}\ \ y=H\Rightarrow T=T_c$$

And other remaining pars on the wall

$$y=H\Rightarrow\frac{\partial T}{\partial y}=0$$

Dimensionless parameters are defined as:

$$X = \frac{x}{H},\ Y = \frac{y}{H},\ U = \frac{u H}{\alpha_f},\ V = \frac{v H}{\alpha_f},\ P = \frac{p H^2}{\rho_{hnf} \alpha_f^2}$$

$$\theta = \frac{T - T_c}{\Delta T},\ C_T = \frac{T_c}{\Delta T},\ \Delta T = \frac{q'' H}{K_f},\ Ec = \frac{\alpha_f^2}{H^2 \left(c_p\right)_f \Delta T}$$

Using those in Eqs. (1) - (5), then non-dimensional form of conservation equations become [67–69]:

$$\frac{\partial U}{\partial X} + \frac{\partial V}{\partial Y} = 0 \tag{6}$$

$$\frac{1}{\varepsilon^2}\left(u \frac{\partial U}{\partial X} + V \frac{\partial U}{\partial Y} \right) = -\frac{\partial P}{\partial X} + \tag{7}$$

$$Pr\left(\frac{\alpha_{hnf}}{\alpha_f} \right)\left(\frac{1}{\varepsilon}\nabla^2 U - \frac{U}{Da} \right) + \frac{(\rho\beta)_{hnf}}{\rho_{hnf}\beta_f} Ra\, Pr \sin\Phi \cdot \theta$$

$$\frac{1}{\varepsilon^2}\left(U \frac{\partial V}{\partial X} + V \frac{\partial V}{\partial Y} \right) = -\frac{\partial P}{\partial Y} + \tag{8}$$

$$Pr\left(\frac{\alpha_{hnf}}{\alpha_f} \right)\left(\frac{1}{\varepsilon}\nabla^2 V - \frac{V}{Da} \right) + \frac{(\rho\beta)_{hnf}}{\rho_{hnf}\beta_f} Ra\, Pr \cos\Phi \cdot \theta -$$

$$Ha^2\, Pr\left(\frac{\sigma_{hnf}}{\sigma_f} \right)\left(\frac{\rho_f}{\rho_{hnf}} \right) V$$

$$\frac{1}{\varepsilon}\left(U \frac{\partial \theta}{\partial X} + V \frac{\partial \theta}{\partial Y} \right) = -\frac{\alpha_{eff,hnf}}{\alpha_{eff,f}} + \tag{9}$$

$$\left(\frac{\partial^2 \theta}{\partial X^2} + \frac{\partial^2 \theta}{\partial Y^2} \right) + \frac{\left(\rho c_p\right)_f}{\varepsilon \left(\rho c_p\right)_{hnf}} Q\, \theta$$

where:

$$Pr = \frac{\nu_f}{\alpha_{eff,f}},\quad Ra = \frac{g\beta_f \Delta T H^3}{\nu_f \alpha_f},\ Ha = B_0 H\sqrt{\sigma_f/\mu_f},\ Da = K/H^2,$$
$$Q = \frac{Q_0 H^2}{(\rho c_p)_f \cdot \alpha_f},\ B = \frac{b}{H},\ D = \frac{d}{H}$$

in Eq. (9) $\alpha_{eff,hnf}$ and $\alpha_{eff,f}$ are equal to:

$$\alpha_{eff,hnf} = -\frac{k_{eff,hnf}}{\left(\rho c_p\right)_{hnf}} \tag{10}$$

$$\alpha_{eff,f} = -\frac{k_{eff,f}}{\left(\rho c_p\right)_f} \tag{11}$$

where

$$k_{eff,hnf} = \varepsilon k_{hnf} + (1-\varepsilon) k_s \tag{12}$$

$$k_{eff,f} = \varepsilon k_f + (1-\varepsilon) k_s \tag{13}$$

Assuming a thermal equilibrium condition, for the validity of Eqs. (12) - (13), the thermal conductivity of the solid phase and the liquid phase must be close to each other. [70]. As a result, this practical principle is considered in this simulation. Also, boundary conditions (Eqs. (6) - (9)) in the dimensionless form are equal to:

$$X = 0, X = 1, Y = 0, Y = 1 \Rightarrow U = V = 0. \tag{14}$$

$$(D - 0.5B) \le X \le (D + 0.5B) \text{ and } Y = 0 \Rightarrow \frac{\partial \theta}{\partial Y} = -\frac{k_{eff,f}}{k_{eff,hnf}}$$

Other remaining parts on the wall

$$Y = 0 \Rightarrow \frac{\partial \theta}{\partial Y} = 0,\ X = 0,\ H \Rightarrow \frac{\partial \theta}{\partial X} = 0$$

$$(D - 0.5B) \le X \le (D + 0.5B) \text{ and } Y = 1 \Rightarrow \theta = 0$$

And other remaining pars on the wall

$$Y = 1 \Rightarrow \frac{\partial \theta}{\partial Y} = 0$$

The local Nusselt number is defined as:

$$Nu_s = \frac{hH}{k_f} = \frac{q'' H}{k_f (T - T_c)} \tag{15}$$

Upon substituting ΔT *and* θ into Eq. (15), the local Nusselt number and average Nusselt number can be written as [67]:

$$Nu_s = \frac{1}{(\theta)_{\text{heat source wall}}} \tag{16}$$

$$Nu_m = \frac{1}{B}\int_{D-0.5B}^{D+0.5B} Nu_s dX \tag{17}$$

The local entropy generation of hybrid nanofluid within porous media under influence of the MHD effect is calculated from the following equation [71]:

$$s = \left(\frac{k_{eff,hnf}}{T^2}\right)\left[\left(\frac{\partial T}{\partial x}\right)^2 + \left(\frac{\partial T}{\partial y}\right)^2\right] + \tag{18}$$
$$\left(\frac{\mu_{hnf}}{T}\right)\left\{\frac{1}{K}(u^2 + v^2) + 2\left[\left(\frac{\partial u}{\partial x}\right)^2 + \left(\frac{\partial v}{\partial y}\right)^2\right] + \left(\frac{\partial u}{\partial y} + \frac{\partial v}{\partial x}\right)^2\right\} +$$
$$\left(\frac{\sigma_{hnf}}{T}\right) B_0^2 v^2$$

According to dimensionless parameters, the entropy generation in non-dimensional form becomes:

$$S = s.\frac{H^2}{k_f} = \left(\frac{k_{eff,hnf}}{k_f(\theta + C_T)^2}\right)\left[\left(\frac{\partial\theta}{\partial X}\right)^2 + \left(\frac{\partial\theta}{\partial Y}\right)^2\right] + \quad (19)$$

$$Ec.\,Pr.\left(\frac{\mu_{hnf}}{\mu_f(\theta + C_T)}\right)\left\{\frac{1}{Da}(U^2 + V^2) + \left[2\left(\left(\frac{\partial U}{\partial X}\right)^2 + \left(\frac{\partial V}{\partial Y}\right)^2\right) + \left(\frac{\partial V}{\partial X} + \frac{\partial U}{\partial Y}\right)^2\right]\right\} +$$

$$Ec.\,Pr.\,H\,a^2.\left(\frac{\sigma_{hnf}}{\sigma_f(\theta + C_T)}\right).V^2$$

Where $C_T = \frac{T_c}{\Delta T}$ and $Ec = \frac{\alpha_f^2}{H^2(c_p)_f \Delta T}$ are the temperature ratio and the Eckert number, respectively. Also, the following ratio of non-dimensional parameters is defined as [62]:

$$Nu_m^{+} = \frac{Nu_m}{(Nu_m)_{\square=0}}, \quad (20)$$

$$Nu_m{}^{++} = \frac{Nu_m}{(Nu_m)_{Ha=0}}, \quad Nu_m{}^{+++} = \frac{Nu_m}{(Nu_m)_{\Phi=0}}$$

$$S^{+} = \frac{S}{(S)_{\square=0}}, \; S^{++} = \frac{S}{(S)_{Ha=0}} \quad (21)$$

$$S^{+++} = \frac{S}{(S)_{\Phi=0}}$$

$$e^{+} = \frac{S^{+}}{Nu_m{}^{+}}, \; e^{++} = \frac{S^{++}}{Nu_m{}^{++}} \quad (22)$$

$$e^{+++} = \frac{S^{+++}}{Nu_m^{+++}}$$

Thermophysical properties of hybrid nanofluid

According to the literature reviews, the effective properties of the Al_2O_3-Cu/water hybrid nanofluid are defined as follows. Assuming the homogeneous mixture model for common nanofluid [12, 62], the density of hybrid nanofluid is specified by [72]:

$$\rho_{hnf} = \phi_{Al_2O_3}\rho_{Al_2O_3} + \phi_{Cu}\rho_{Cu} + (1-\phi)\rho_{bf} \quad (23)$$

where ϕ is equal to:

$$\phi = \phi_{Al_2O_3} + \phi_{Cu} \quad (24)$$

Similar to the heat capacitance of the nanofluid [73], the heat capacity of hybrid nanofluid can be expressed:

$$\left(\rho C_p\right)_{hnf} = \phi_{Al_2O_3}\left(\rho C_p\right)_{Al_2O_3} + \quad (25)$$

$$\phi_{Cu}\left(\rho C_p\right)_{Cu} + (1-\phi)\left(\rho C_p\right)_{bf}$$

Also, thermal expansion of hybrid nanofluid can be defined as follows:

$$(\rho\beta)_{hnf} = \phi_{Al_2O_3}(\rho\beta)_{Al_2O_3} + \phi_{Cu}(\rho\beta)_{Cu} + \quad (26)$$

$$(1-\phi)(\rho\beta)_{bf}$$

According to the Maxwell-Garnetts model [74–76] and effective dynamic viscosity Brinkman model [77] for the thermal conductivity and effective dynamic viscosity of the common nanofluid, respectively, these properties can be obtained for hybrid nanofluid as [76]:

$$\frac{k_{hnf}}{k_{bf}} = \left\{\frac{\left(\phi_{Al_2O_3}k_{Al_2O_3} + \phi_{Cu}k_{Cu}\right)}{\phi} + 2k_{bf} + \quad (27)\right.$$

$$2\left(\phi_{Al_2O_3}k_{Al_2O_3} + \phi_{Cu}k_{Cu}\right) + 2\phi k_{bf}\Big)\times$$

$$\left\{\frac{\left(\phi_{Al_2O_3}k_{Al_2O_3} + \phi_{Cu}k_{Cu}\right)}{\phi} + 2k_{bf} - \right.$$

$$\left.\left(\phi_{Al_2O_3}k_{Al_2O_3} + \phi_{Cu}k_{Cu}\right) + \phi k_{bf}\right)^{-1}$$

$$\mu_{hnf} = \frac{\mu_{bf}}{\left(1 - \left(\phi_{Al_2O_3} + \phi_{Cu}\right)\right)^{2.5}} \quad (28)$$

and hybrid nanofluid thermal diffusivity can be defined as:

$$\alpha_{hnf} = \frac{k_{hnf}}{(\rho C_p)_{hnf}} \quad (29)$$

from the Maxwell model [74] for effective electrical conductivity of nanofluid, the effective electrical conductivity of hybrid nanofluid can be obtained:

$$\frac{\sigma_{\square nf}}{\sigma_{bf}} = 1 + \quad (30)$$

$$\frac{3\left(\frac{(\phi_{Al_2O_3}\sigma_{Al_2O_3} + \phi_{Cu}\sigma_{Cu})}{\sigma_{bf}} - \left(\phi_{Al_2O_3} + \phi_{Cu}\right)\right)}{\left(\frac{(\phi_{Al_2O_3}\sigma_{Al_2O_3} + \phi_{Cu}\sigma_{Cu})}{\phi\sigma_{bf}} + 2\right) - \left(\frac{(\phi_{Al_2O_3}\sigma_{Al_2O_3} + \phi_{Cu}\sigma_{Cu})}{\sigma_{bf}} - \left(\phi_{Al_2O_3} + \phi_{Cu}\right)\right)}$$

The characteristics of Cu and Al_2O_3 nanoparticles and water are presented in Table 1.

In this investigation, the weight proportions of Al_2O_3 and Cu have been taken in the same ratio as 50:50.

Solution methodology

Various computational methods have been used for studying heat transfer and fluid flow inside cavities and enclosures [80-81]. In the present study, the finite difference method is used for solving the governing

Table 1: Characteristics of water, Copper, and Alumina.

Property	Water	Copper (Cu)	Alumina (Al_2O_3)
ρ (kg/m^3) [78]	997.1	8933	3970
C_p (J/kg.K) [78]	4179	385	765
k (W/m.K) [78]	0.613	401	40
β (K^{-1}) [79]	21×10^{-5}	1.67×10^{-5}	0.85×10^{-5}
σ (μS/cm) [67]	0.05	$5.96 \times 10^{+7}$	1×10^{-10}

Table 2: Comparison of the average Nusselt number Num for $B = 0.4$, $\phi = 0.1$, $D = 0.5$

Ra	Aminossadati and Ghasemi [88]	Present
10^3	5.451	5.450
10^4	5.474	5.475
10^5	7.121	7.204
10^6	13.864	14.014

equations (6)-(9) with the boundary conditions (14) which are based on the finite-difference methodology [82–87]. Central difference quotients are used to approximate the second derivatives in both the *X* and *Y* directions. Hence, the obtained discretized equations have been solved utilizing the Successive Under-Relaxation (SUR) method as the following algorithm:

(a) Select a suitable grid. A grid 21×21 is a good start in many cases.

(b) All dependent variables are initialized to zero.

(c) The new boundary values at (*n*+1) are computed for all walls from the previous values at (*n*).

(d) The new temperature and the new stream function at (*n*+1) are computed from previous (*n*) values at all internal grid points.

(e) The velocity components *U* and *V* are computed calculated at (*n*+1) from the values at (*n*) explicitly for all the internal grid points.

(f) The same procedure is followed by starting with step (c) to obtain the solution at the next time step at (*n*+2).

(h) The appropriate value of the relaxation parameter is found to be equal 0.7 and the iteration process is terminated if the following condition satisfies: $\sum_{i,j}\left|\chi_{i,j}^{new} - \chi_{i,j}^{old}\right| \leq 10^{-7}$, where χ is the general dependent variable which can stand for *U*, *V*, or θ, and *n* denotes the iteration step. For verification of code the grids sensitivity study with four sets of grids: 41×41, 61×61,81×81, and 101×101 is done. A good agreement is found between (81×81) and (101×101) grids, so the numerical computations are carried out for (81×81) grid nodal points.

In order to check the accuracy of the present method, the obtained results are compared in special cases (B= 0.4, ϕ= 10%, D= 0.5) with the results obtained by Aminossadati and Ghasemi [88]. These comparisons are presented clearly in Fig. 2 and Table 2 in terms of the average Nusselt number at the heat source. A very good agreement is found between the results.

Also, taking into account the MHD influence, *Sheikholeslami et al.* [89] have examined the natural convection of Cu-water nanofluids in a square cavity. In the investigation of *Sheikholeslami et al.* [89], the upper wall of the cavity was well insulated while the vertical side walls were at a constant temperature T_c. The lower wall was partially heated which was at a constant temperature T_h. According to the boundary condition and notation of *Sheikholeslami et al.* [89], the Nusselt number was performed as 9.429 when Ra=10^5, ε=0.8 (the bottom flash element length), ϕ=0.04, and Ha=100. Here, we obtained the Nusselt number as 9.4286 which exhibits a very good agreement with the literature value.

RESULTS AND DISCUSSION

The results are obtained at the fixed parametric values: $Da = 10^{-3}$, $\varepsilon = 0.5$, $Pr = 6.2$, $Ec = 10^{-3}$and $C_T = 0.5$ and various main parameters: hybrid nanofluid volume fraction ($0 \leq \phi \leq 0.1$, Rayleigh number ($10^2 \leq Ra \leq 10^6$), Hartmann number ($0 \leq Ha \leq 50$), angle of enclosure ($0° \leq \Phi \leq 360°$), internal heat generation/absorption ($-2 \leq Q \leq 2$), heat sink and source size ($0.2 \leq B \leq 0.8$), and heat sink and source location ($0.3 \leq D \leq 0.7$). The results are represented in various terms such as streamlines, isotherms, Nusselt number, entropy generation, and thermal performance distribution. Also, the variation of ration parameters is illustrated.

The effect of hybrid nanofluid volume fraction

Fig. 3 manifests the impacts of the boost in the hybrid nanofluid volume fraction on the streamlines and isotherms lines. Such impacts are more on the isotherms lines than on the streamlines. As elucidated in this figure, the isothermal lines move to the left of the heat source with the increase in the hybrid nanofluid volume fraction, and hence, at a certain section, the temperature rises with the increase of nanoparticle concentration.

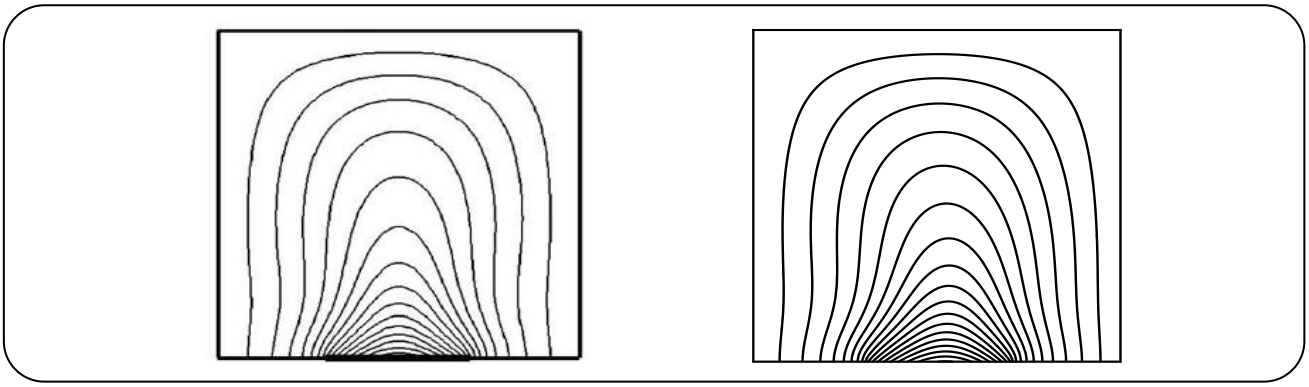

Fig. 2: Comparison of the current isotherms (right) and those obtained by Aminossadati and Ghasemi [88] (left) at B=0.4, Ra = 10^5, ϕ = 0.1 and D = 0.5.

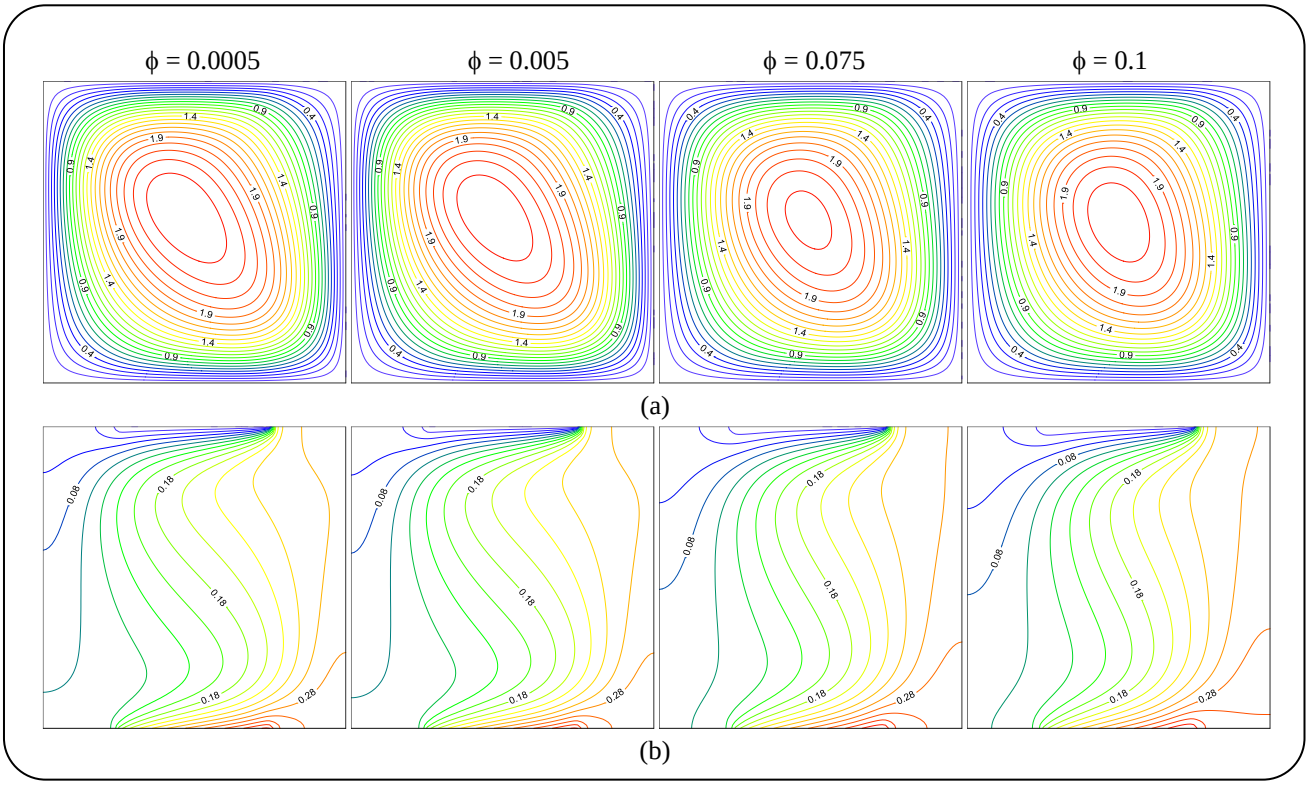

Fig. 3: Streamlines (a) and Isothermal (b) for Al_2O_3–Cu/water Hybrid Nanofluid at Ha = 10, Q = 1, D = 0.5, B = 0, Φ = 15° = Ra = 10^5, Da = 10^{-3}, ε = 0.5.

Considering the definition of the Nusselt number, the amount of the Nusselt number diminishes. On the other hand, by moving from the left to the right side of the source, the temperature increases for all amounts of ϕ, and the local Nusselt number, therefore, decreases continuously. So that, the Nu_m and $Nu_m{}^{++}$ decrease with hybrid nanofluid volume fraction increment as shown in Fig. 4-a and 4-b. Also, it is observed that increasing the magnetic field intensity has a similar effect. Fig. 4 indicates that the Nu_m decreases by the increase of the Ha number because the Lorentz force induced opposite body force against the bouncy force and it is distinctive for the stronger magnetic field. Also, for different Hartmann numbers, the Nu_m decreases as the volume fraction rise. Enhancing dynamic viscosity because adding the nanoparticles to pure fluid tends to induce more resistance due to shear forces against the fluid motion and decrease the fluid velocities and directly reduce the heat transfer

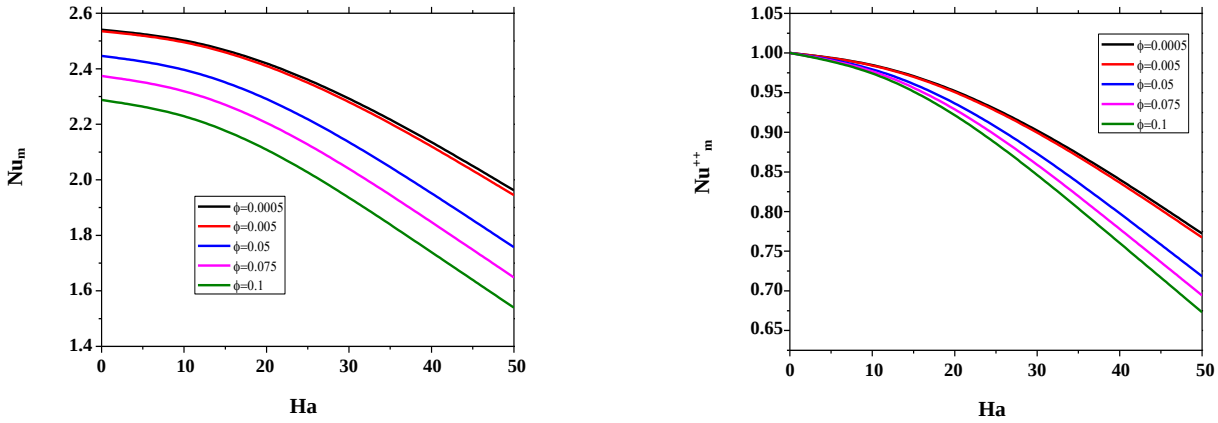

Fig.4: Variation of the average Nusselt number with Hartmann number at Q = 1, D = 0.5, B = 0.5, Φ = 15°, Ra = 10^5, Da = 10^{-3}, ε = 0.5.

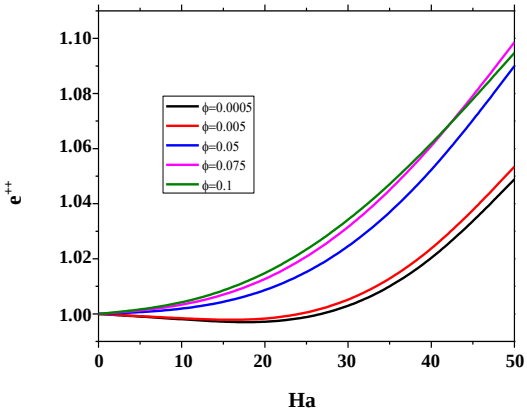

Fig. 5: Variation of e++ at various hybrid nanofluid volume fraction Q = 1, D = 0.5, B = 0.5, Φ = 15°, Ra = 10^5, Da = 10^{-3}, ε = 0.5.

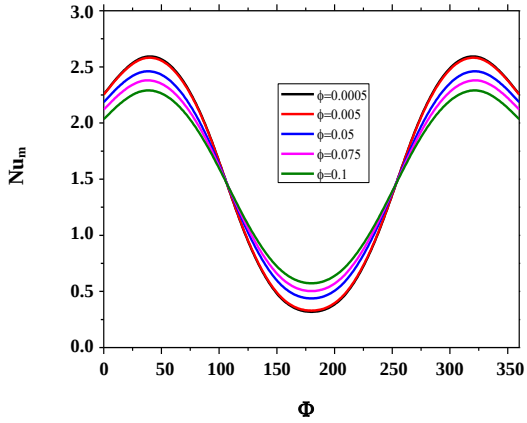

Fig. 6: Variation of the average Nusselt number via Φ at Ha = 10, Q = 1, D = 0.5, B = 0.5, Ra = 10^5, Da = 10^{-3}, ε = 0.5.

By the reduction of the advection mechanism. Despite the increase in conductivity of nanofluid, but some cases of natural heat transfer the viscosity affects heat transfer more than conductivity.

As exhibited in Fig. 5, the thermal performance increases more in the case of high volume fraction and high Hartmann number in comparison with low concentration and low Hartmann number. Fig. 6 manifests the average Nusselt number for different values of the volume fraction and the cavity angle. As evident in the figure, the maximum values of the Nusselt number occur in the first and fourth quarters of the trigonometric circle. In these regions, the average Nusselt number falls down by adding hybrid nanoparticles. A peak in the Nusselt number is also observed in these quarters occurring because of the temperature gradient. In the second quarter, the average Nusselt number reduces due to cavity angle increment and increases by adding hybrid nanoparticles to the base fluid. In the third quarter, the addition of hybrid nanoparticles accounts for more heat transfer. Because the adiabatic walls, heat sink, and heat source are at the upper and lower side of the cavity and equal values on the sides of degree=180°, the curves seem to be symmetric at about degree=180°. The variation of average entropy generation with cavity angle in the first and third quarter has the same behavior as the Nusselt number but in the second quarter reduced by the increasing amount of hybrid nanoparticles in the base fluid as shown in Fig. 7.

The effect of Rayleigh number

Fig. 8 depicts the impact of the Rayleigh number on the streamlines and isotherms. As the Rayleigh number rises, the streamlines become stronger. Furthermore, their

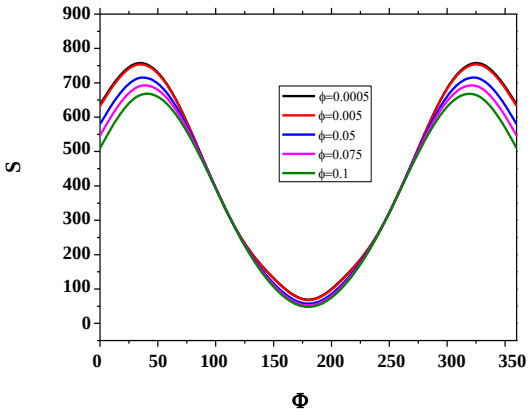

Fig. 7: Variation of the average total entropy generation ratio via Φ at Ha = 10, Q = 1, D = 0.5, B = 0.5, Ra = 10^5, Da = 10^{-3}, ε = 0.5.

the elliptical core rotates 90 degrees and becomes more elongated. The increase of the Rayleigh number also makes the nearly horizontal isothermal lines tend to become vertical because of increasing the buoyancy effects due to the enhancement of Ra number. As shown in isotherms the value of temperature near the heat source decreases via increasing Ra number so the Nu number experiences more value at a high Ra number. Also considering the definition of the Nusselt number, the amount of the local Nusselt number diminishes except for Ra=10^2 and 10^3.

For Rayleigh number greater than 10^3, from the left side of the source to the right side, the temperature increases, and the Nusselt number, therefore, decreases continuously as shown in Fig. 9. Fig. 10 shows the variation of the Nu_m^+ via increasing the Rayleigh number. As illustrated in Fig. 10, for Ra numbers 10^2 and 10^3, the addition of nanoparticles leads to increments of the Nusselt number. This effect can be seen in Fig. 8-b that isotherms are parallel to the heat source at Ra=10^2 and 10^3. The rate of growth at Ra=10^6 is less than that of the above-mentioned Ra. The Nu_m lessens by the addition of nanoparticles at Ra=10^4. For increasing the heat transfer, it is recommended to add nanoparticles to the pure fluid in two low Ra numbers. Fig. 11 indicates that the addition of nanoparticles for different Rayleigh numbers causes the thermal performance to be declined. This happens more at Ra=10^2 and 10^3 compared with other values of the Ra. At Ra=10^6, the optimum value of thermal performance occurs when hybrid nanoparticles are added. As shown in Fig. 8, Rayleigh numbers increasing the lead to the augmentation of the temperature gradient and more entropy generation.

The effect of heat generation/absorption

Fig. 12 describes the influence of internal heat generation/absorption on the streamlines and isotherms. With the increase of Q and accordingly the internal heat generation, the streamlines get stronger and rotate in the CCW direction with a higher velocity. For a negative value of Q, the isothermal lines are slant. As Q increases, and gets positive values, such lines become nearly vertical. It is worth noting that around the heat sink, the density of the isothermal lines at Q=-2 is high. As observed in isothermal lines near the heat source, the temperature rises with the increase of Q at a fixed point, and hence, the Nusselt number lowers (can be seen in Fig. 13) considering its definition. Besides, when Q is constant, the temperature and the Nusselt number decrease as moving from the beginning to the end of the heat source. As observed in Fig. 14, the increase of hybrid nanoparticles concentration leads to the decrease of the normalize Nusselt number (normalized to the case of ϕ=0). The rate of reduction is more for Q=-2 and less for positive values of Q than other Q values. Fig. 15 demonstrates the variations of the Nu_m for a range of values of cavity angles and Q. For all values, the sinusoidal pattern is obvious in this figure. Generally, by the increase of Q, from negative values to positive ones, the Nusselt number is reduced.

Variations of the normalized entropy generation (S^+) for different values of Q and volume fractions are presented in Fig. 16. In general, the addition of nanoparticles leads to the reduction of the entropy generation. The rate of reduction is maximum at Q=-2, and is minimum at Q=2. Fig. 17 shows that the S^{++} decreases with the Hartmann number. As can be seen, the S^{++} decreases with the Hartmann number which has a sharper rate at Q=-2 compared to Q=2. This means heat absorption has a higher impact on the production of entropy than heat generation.

Fig. 18 exhibits the effect of adding nanoparticles on the thermal performance for different values of Q. such addition accounts for the maximum reduction of the thermal performance at Q=-2 and the minimum reduction rate at Q=2. As evident in Fig. 19, for positive values of Q, the thermal performance is improved when the Hartmann number rises, having a positive impact on the thermal

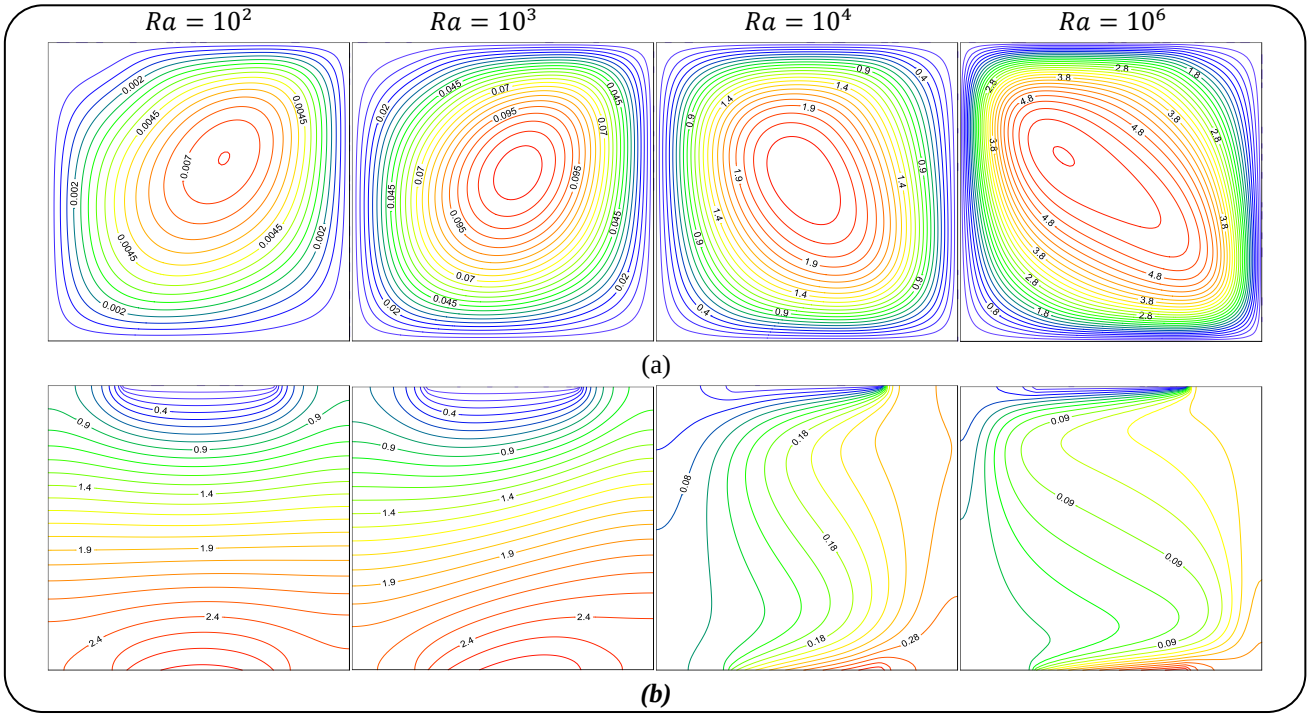

Fig. 8: Streamlines (a) and Isothermal (b) versus Rayleigh number at ϕ = 0.05, Ha = 10, Q = 1, D = 0.5, B = 0.5, Φ = 15°, Da = 10^{-3}, ε = 0.5.

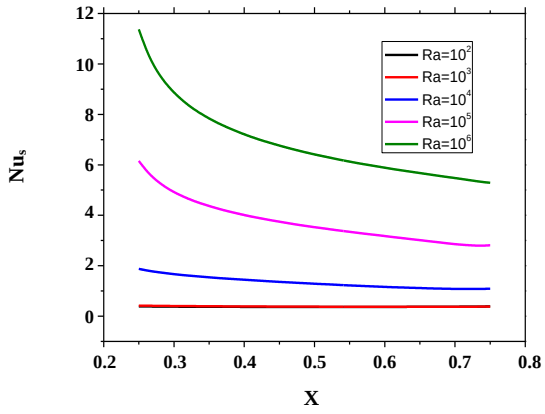

Fig. 9: Profiles of the local Nusselt number along the heat source in various Ra at Ha = 10, Q = 1, D = 0.5, B = 0.5, Φ = 15°, Da = 10^{-3}, ε = 0.5.

performance criteria. Conversely, the thermal performance lowers with the increase of the Hartmann number for negative values of Q.

The effect of heat sources length and location

The effect of the heat source length (B) on the streamlines and isotherms is illustrated in Fig. 20 for the centered heat source location ($D = 0.5$). As can be seen in Fig. 20-a, increasing the heat source length leads to stronger circulation around it. On the other hand, the isotherms presented in Fig. 20-b are influenced by the heat flux length as expected. The isotherms become more stratified for a higher heat source length. As can be seen from the isotherms, the temperature gradient near the bottom and top walls have the highest values at the edges of the heat source.

Fig. 21 shows the local Nusselt numbers for different heat sources length along the heat source at D = 0.5. As shown in Fig. 20-b, by increasing B, a higher temperature gradient near the heat source happens which leads to a higher Nusselt number for larger heat source lengths. Moreover, the normalize Nusselt numbers for different hybrid nanoparticle volume fractions and Hartmann number are presented in Figs. 22-23 against various B. The Nu^+ lowers with the hybrid nanoparticle volume fraction. The effect of the volume fraction on the Nu^+ reduces with increasing the heat flux length. As clarified in Fig. 23, for a constant heat source length, the Nu^{++} decreases by the increase of the Hartmann number. This occurs due to the reduction of buoyancy force because of the generation of strong Lorentz force. For a constant Hartmann number, increasing B also leads to the increment of the Nu^{++}.

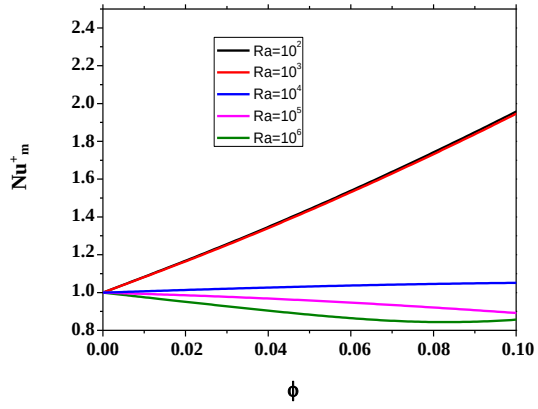

Fig. 10: Variation of the average Nusselt number via hybrid nanofluid volume fraction at Ha = 10, Q = 1, D = 0.5, B = 0.5, $\Phi = 15°$, Da = 10^{-3}, $\varepsilon = 0.5$.

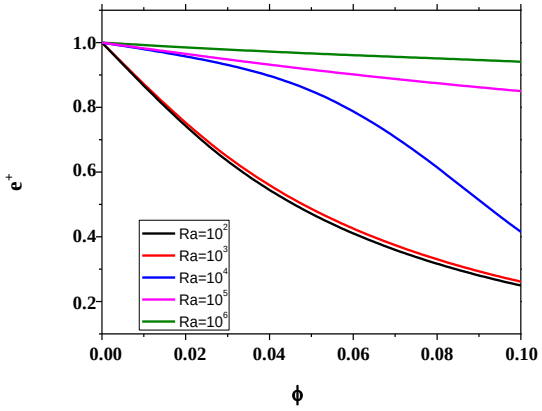

Fig. 11: Variation of e+ via increasing hybrid nanofluid volume fraction in various Rayleigh number at Ha = 10, Q = 1, D = 0.5, B = 0.5, $\Phi = 15°$, Da = 10^{-3}, $\varepsilon = 0.5$.

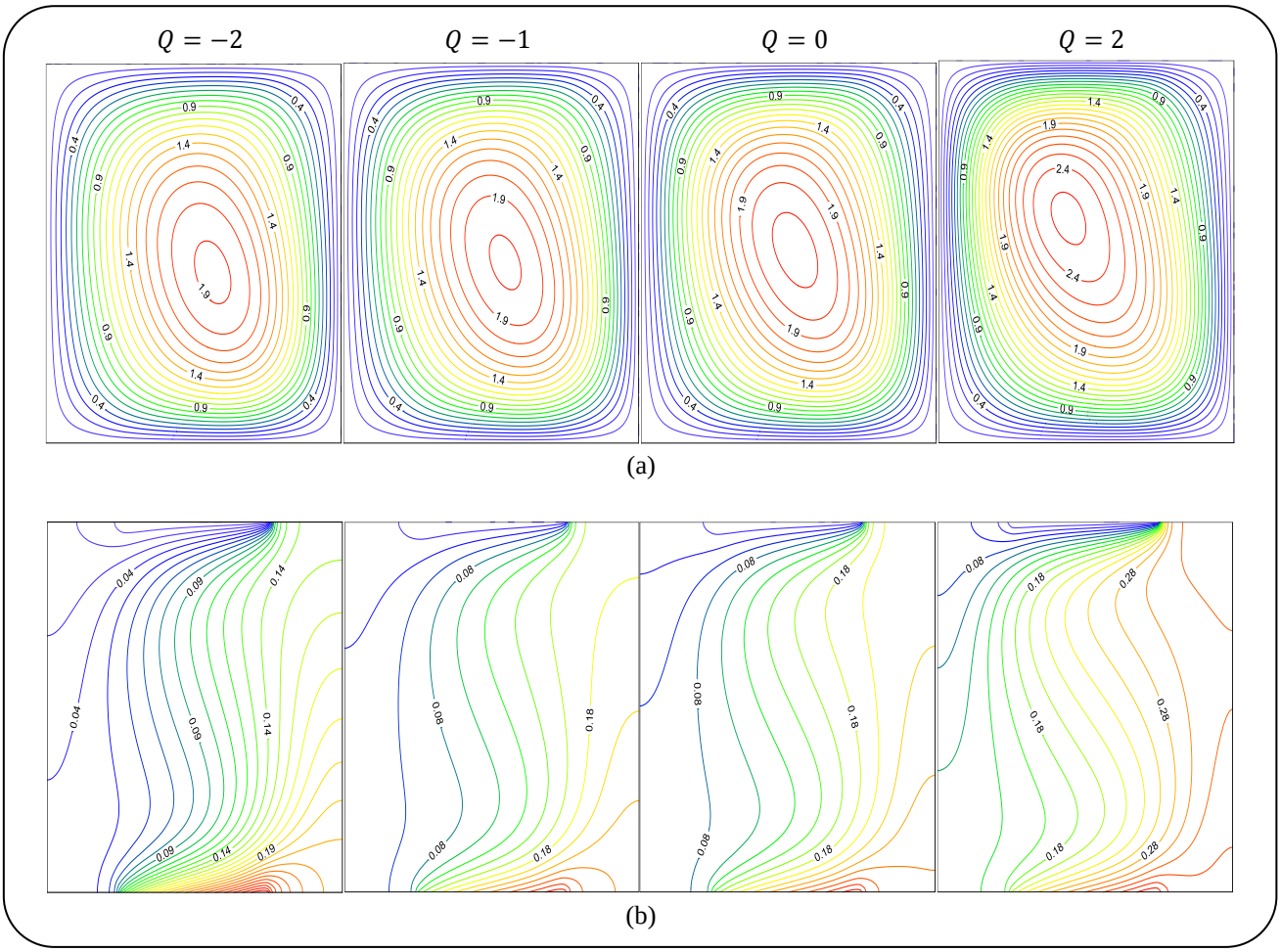

Fig. 12: Streamlines (a) and Isothermal (b) for Al_2O_3–Cu/water Hybrid Nanofluid at $\phi = 0.05$, Ha = 10, Ra = 10^5, D = 0.5, B = 0.5, $\Phi = 15°$, Da = 10^{-3}, $\varepsilon = 0.5$.

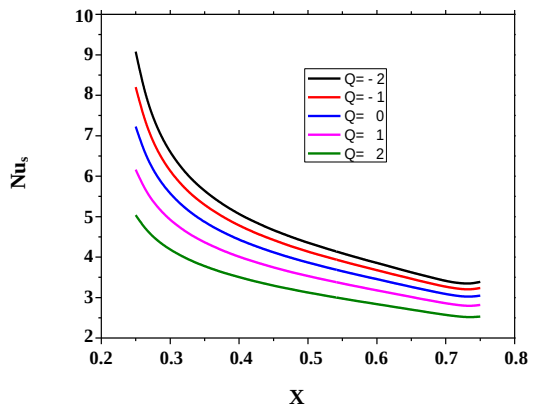

Fig. 13: Profiles of the local Nusselt number along the heat source in various Q at $\phi = 0.05$, Ha = 10, Ra = 10^5, D = 0.5, B = 0.5, $\Phi = 15°$, Da = 10^{-3}, $\varepsilon = 0.5$.

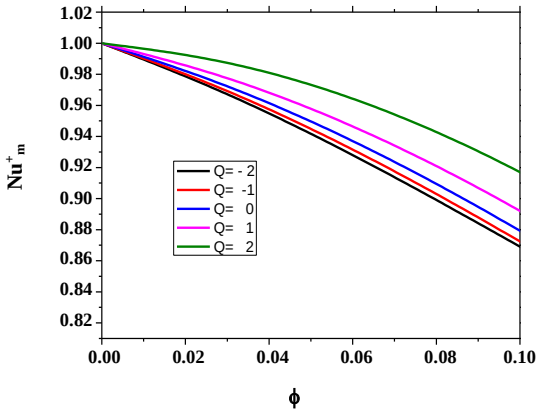

Fig. 14: Variation of the average Nusselt number via changing hybrid nanofluid volume fraction and Q at Ha = 10, Ra = 10^5, D = 0.5, B = 0.5, $\Phi = 15°$, Da = 10^{-3}, $\varepsilon = 0.5$.

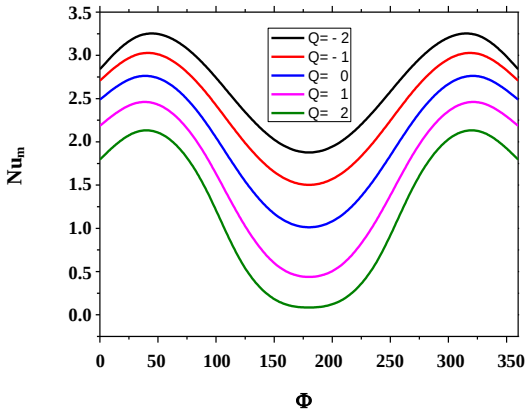

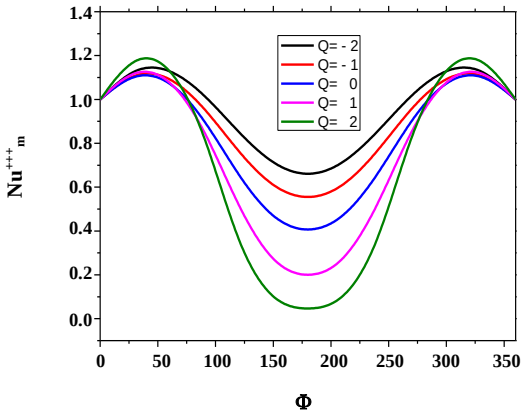

Fig. 15: Variation of the average Nusselt number via Φ at $\phi = 0.05$, Ha = 10, Ra = 10^5, D = 0.5, B = 0.5, Da = 10^{-3}, $\varepsilon = 0.5$.

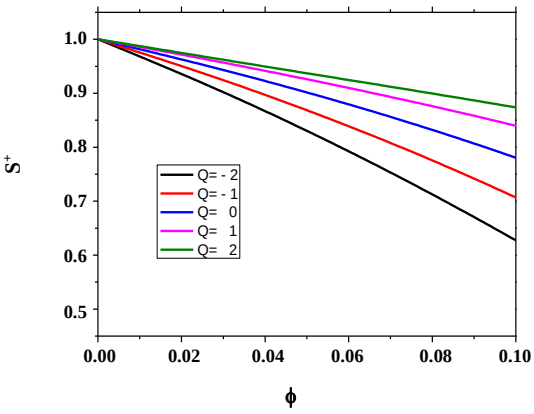

Fig. 16: Global entropy generation ratio via Q and volume fraction at Ha = 10, Ra = 10^5, D = 0.5, B = 0.5, $\Phi = 15°$, Da = 10^{-3}, $\varepsilon = 0.5$.

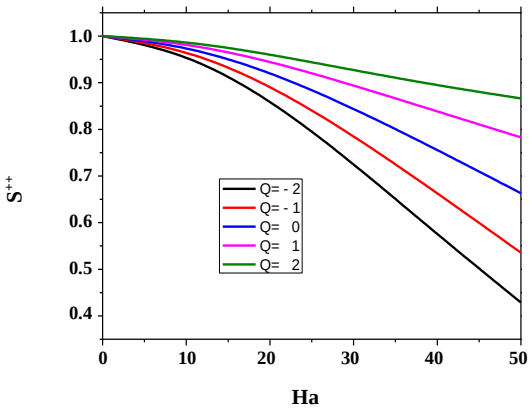

Fig. 17: Local entropy generation at $\phi = 0.05$, Ra = 10^5, D = 0.5, B = 0.5, $\Phi = 15°$, Da = 10^{-3}, $\varepsilon = 0.5$.

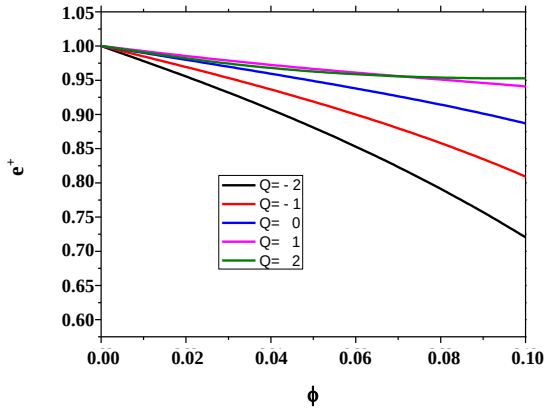

Fig. 18: Variation e^{+} with changing Q at Ha = 10, Ra = 10^5, D = 0.5, B = 0.5, Φ = 15°, Da = 10^{-3}, ε = 0.5.

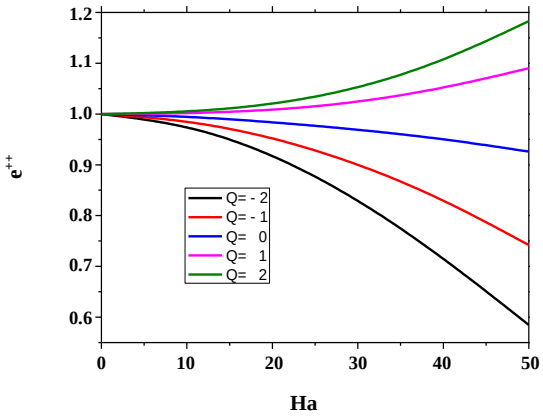

Fig. 19: Variation e^{++} with changing Q at ϕ =0.05, Ra = 10^5, D = 0.5, B = 0.5, Φ = 15°, Da = 10^{-3}, ε = 0.5.

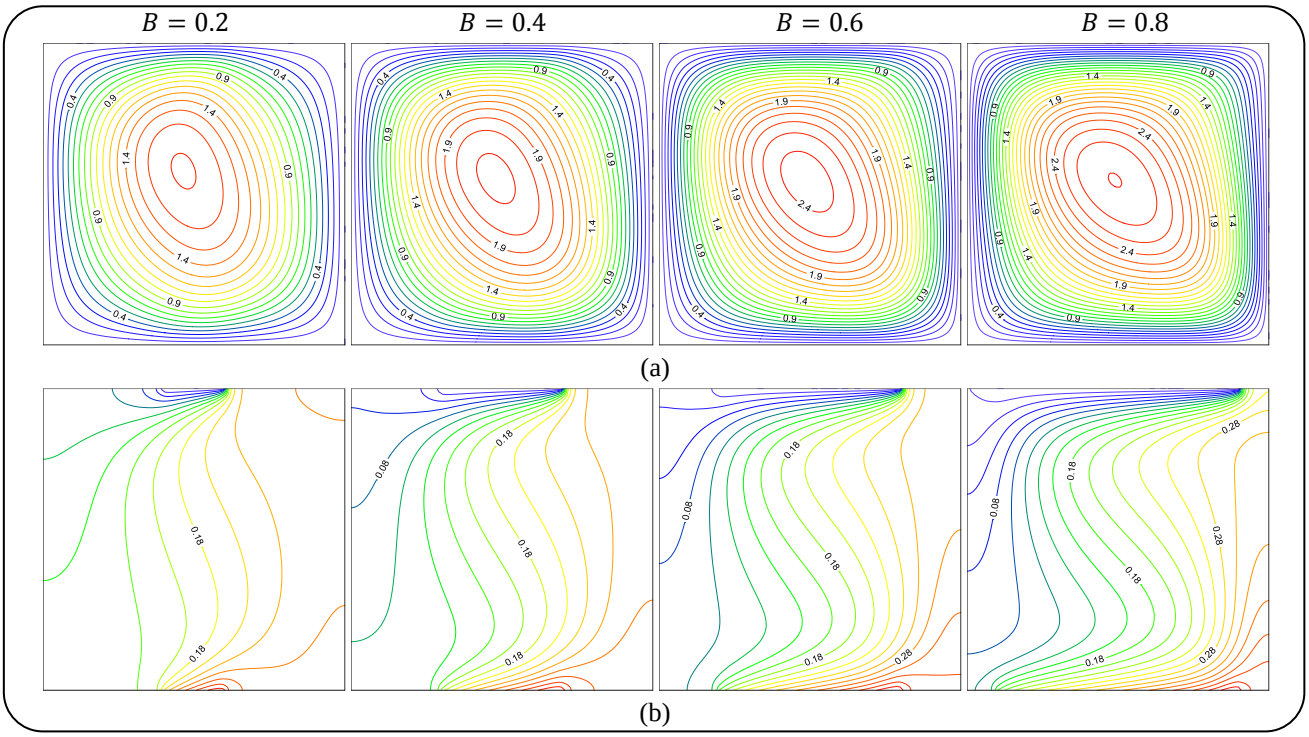

Fig. 20: Streamlines (a) and Isothermal (b) at ϕ = 0.05, Ha = 10, Ra = 10^5, D = 0.5, Φ = 15°, Da = 10^{-3}, ε = 0.5.

As exhibited in Fig. 24, variation of Nu_m with cavity angles showing the sinusoidal pattern at all values of B. It is noticeable that the maximum and minimum values of the Nusselt number are different in the first and third quarters from the second quarter. As clarified in Fig. 25, for a constant heat source length, the S^{++} decreases by the increase of the Hartmann number. This occurs due to the reduction of the heat transfer and the temperature gradient described in the previous figures. For a constant Hartmann number, increasing the B also leads to the reduction of the entropy generation. Fig. 26 demonstrates the influence of volume fraction on e^{+} for different B. As evident in the figure, the increment of the volume fraction leads to the reduction of normalized thermal performance and it is sharper for high heat source length. Fig. 27 demonstrates that e^{++} increases with Ha except for B = 0.8. At B = 0.8, from Ha=0 to Ha=30 normalize thermal performance decreases then it increases. Increasing normalized thermal performance means that the relative decrease in entropy generation is more than the relative decrease in the Nusselt number with an increase in the magnetic field strength.

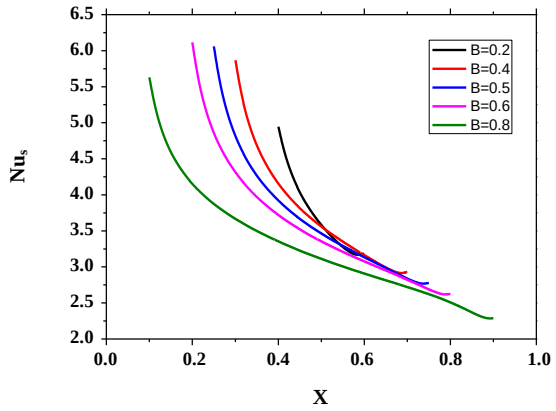

Fig. 21: Profiles of the local Nusselt number along the heat source at ϕ = 0.05, Ha = 10, Ra = 10^5, D = 0.5, Φ = 15°, Da = 10^{-3}, ε = 0.5.

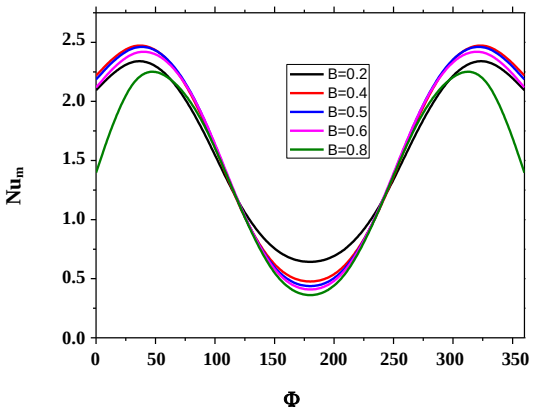

Fig. 24: Variation of the average Nusselt number at ϕ = 0.05, Ha = 10, Ra = 10^5, D = 0.5, Da = 10^{-3}, ε = 0.5.

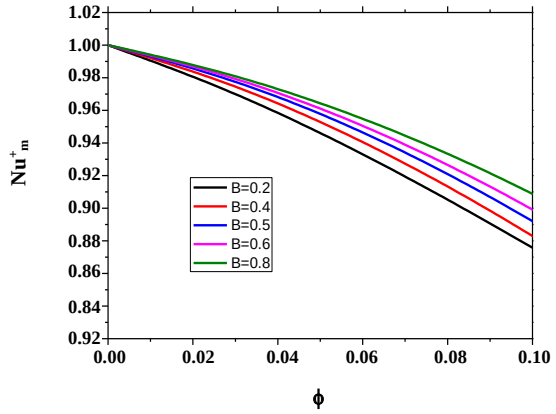

Fig. 22: Variation of the average Nusselt number at Ha =10, Ra = 10^5, D = 0.5, B = 0.5, Φ = 15°, Da = 10^{-3}, ε = 0.5.

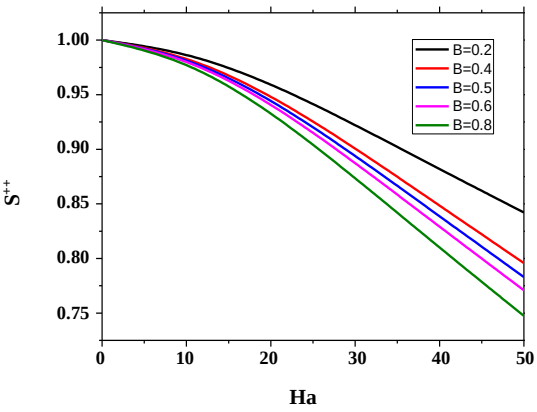

Fig. 25: Global entropy generation ratio via Hartmann number at ϕ = 0.05, Ra = 10^5, D = 0.5, Φ = 15°, Da = 10^{-3}, ε = 0.5.

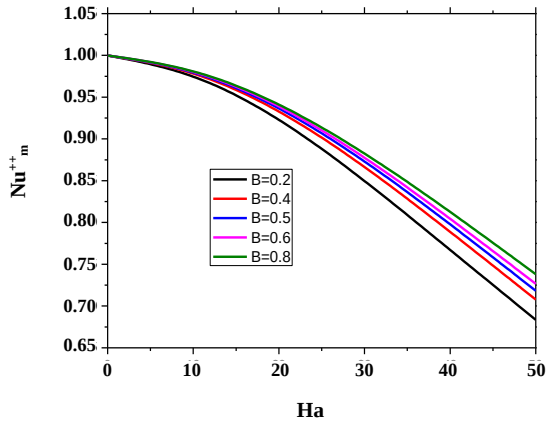

Fig. 23: Variation of the average Nusselt number at ϕ =0.05, Ra = 10^5, D = 0.5, Φ = 15°, Da = 10^{-3}, ε = 0.5.

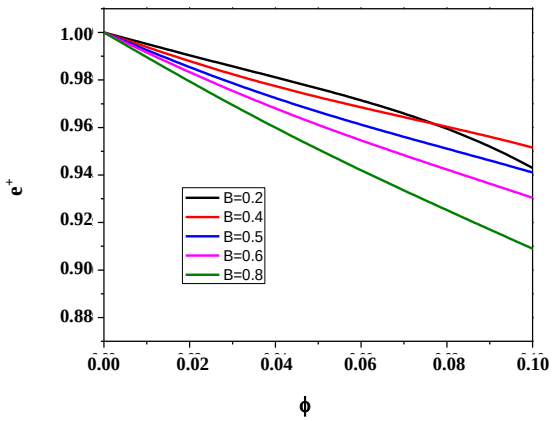

Fig. 26: Global entropy generation ratio at Ha = 10, Ra = 10^5, D = 0.5, Φ = 15°, Da = 10^{-3}, ε = 0.5.

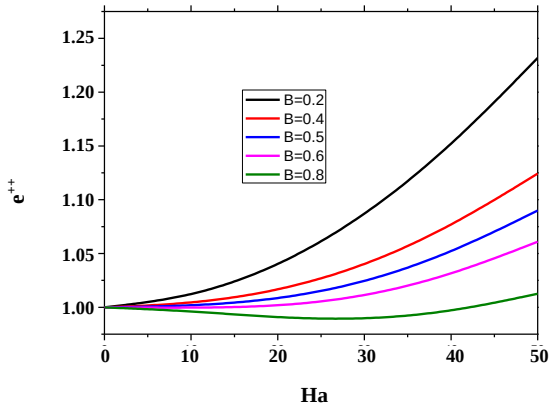

Fig. 27: Global entropy generation ratio via Hartmann number at $\phi = 0.05$, $Ra = 10^5$, $D = 0.5$, $\Phi = 15°$, $Da = 10^{-3}$, $\varepsilon = 0.5$.

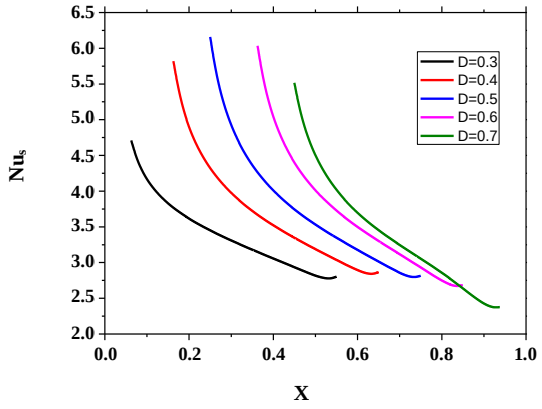

Fig. 28: Profiles of the local Nusselt number along the heat source at $\phi = 0.05$, $Ha = 10$, $Ra = 10^5$, $B = 0.5$, $\Phi = 15°$, $Da = 10^{-3}$, $\varepsilon = 0.5$.

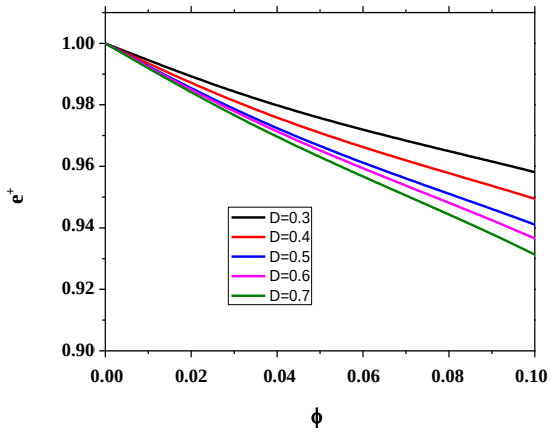

Fig. 29: Global entropy generation ratio at $Ha = 10$, $Ra = 10^5$, $B = 0.5$, $\Phi = 15°$, $Da = 10^{-3}$, $\varepsilon = 0.5$.

The local Nusselt number is presented in Fig. 28 for different heat source locations. It can be seen that the Nusselt number is influenced by changing the heat source location. Similar to the local Nusselt numbers presented in Figs. 9 and 21, the location of the maxima in each curve of Fig. 28 is at the left edges of the source. As shown in Fig. 29, the functionality of normalized thermal performance with the hybrid nanoparticle volume fraction is more pronounced if the heat source is positioned at a higher location. The case of D = 0.5 achieves the highest Nusselt number (Fig. 28), however, as illustrated in Fig. 29, normalized thermal performance varies slightly with the volume fraction for lower D values.

CONCLUSIONS

The impact of volume fraction, Rayleigh number, heat generation, and heat source length and location on magneto-free convective hybrid nanofluid flow inside a slant porous cavity with entropy analysis is studied numerically. Based on the Under-Relaxation (SUR) technique to find the solutions to the non-linear problem, the key conclusions are listed:

1- Increasing hybrid nanoparticles concentration lead to a reduction in Nusselt number.

2- With the enhancement of the Hartmann number for all ranges of ϕ, the average Nusselt number decreases noticeably.

3- The thermal performance reduces more in the case of high volume fraction in comparison with low concentration.

4-The addition of nanoparticles for several Rayleigh numbers causes the thermal performance to be declined.

5- Thermal performance improvement occurred by enhancement of the magnetic field at $Ra=10^3$ and 10^5.

6- Totally, by focusing on thermal performance criteria adding the nanoparticle can be recommended in all Ra numbers, but only for heat transfer adding that is good at $Ra=10^2$ and 10^3

7- In general, the addition of nanoparticles leads to the reduction of entropy generation. The rate of reduction is maximum at Q=-2, and is minimum at Q=2.

8- Generally, by the increase of Q from negative values to positive ones, the Nusselt number is reduced.

However, the novelty of the current simulation is that the magneto-hybrid nanofluid flow inside a slant porous cavity had not been investigated yet, which has been analyzed in the present research work. Further, a new thing is present in the present investigation that deals with the impact

of volume fraction, Rayleigh number, heat generation, heat source length, and location on magneto-free convective hybrid nanofluid flow inside a slant porous cavity with entropy analysis. The results which we obtained in the current study are very productive for improving the performance of roller pumps and cooling electronic devices by using the hybrid nanofluid.

For future work, using LNTE model of porous media is very interesting and closer to reality.

Acknowledgments

The Office of the Vice-Chancellor for Research, Islamic Azad University, Semnan Branch, sponsored, the work of Hadi Kargarsharifabad (The fifth author) with Grant No. 17751-19/11/1395.

Nomenclature

B	Dimensionless of heat source/sink length
B_0	Magnetic field strength, T
b	Length of heat source, m
C_p	Specific heat, J/kg.K
C_T	Dimensionless temperature ratio
D	Dimensionless heat source position
Da	Darcy number
d	Location of heat sink and source, m
Ec	Eckert number
g	Acceleration due to gravity, m/s^2
H	Length of the cavity, m
Ha	Hartmann number
K	Permeability of the porous medium
k	Thermal conductivity, W/m.k
k_{ff}	Effective thermal conductivity of porous media, W/m.k
Na_s	Local Nusselt number
Na_m	Average Nusselt number of heat source
p	Fluid pressure, Pa
P	Dimensionless pressure
Pr	Prandtl number
Q_0	Heat generation coefficient
Ra	Rayleigh number
s	Entropy generation, W/K.m^3
T	Temperature, K
u, v	Velocity components in x, y directions, m/s
U, V	Dimensionless velocity components
x, y	Cartesian coordinates, m
X, Y	Dimensionless coordinates

Greek symbols

α	Thermal diffusivity, m^2/s
β	Thermal expansion coefficient, 1/K
ϕ	Solid volume fraction
σ	Effective electrical conductivity, μS/cm
θ	Dimensionless temperature
μ	Dynamic viscosity, N.s/m^2
ν	Kinematic viscosity, m^2/s
ρ	Density, kg/m^3
Φ	Angle of the enclosure, Degree
ε	Porosity of the porous medium

Subscripts

0	Reference
c	Cold
f	Base fluid
eff,f	Effective property of the base fluid and porous media
eff,hnf	Effective property of hybrid nanofluid and porous media
h	Hot
hnf	Hybrid nanofluid
m	Average
nf	Nanofluid
p	Nanoparticle

Abbreviations

MHD	Magnetohydrodynamic
MWCNT	Multi-walled carbon nanotube
SUR	Successive Under-Relaxation

Received : Sep. 9, 2020 ; Accepted : Dec. 21, 2020

REFERENCES

[1] Kargarsharifabad H., Optimization of Arrangement of Conducting Fins and Insulated Obstacles Inside a Cavity: the Couple of Numerical Solutions and Genetic Algorithm Methods, *J. Therm. Anal. Calorim.* (2020).

[2] Yang R.-J., Hou H.-H., Wang Y.-N., Fu L.-M., Micro-Magnetofluidics in Microfluidic Systems: A Review, *Sensors Actuators B Chem.* **224**: 1–15 (2016).

[3] Chamkha A.J., Selimefendigil F., Oztop H.F., Effects of a Rotating Cone on the Mixed Convection in a Double Lid-Driven 3D Porous Trapezoidal Nanofluid Filled Cavity Under the Impact of Magnetic Field, *Nanomaterials*, **10(3)**: 1–17 (2020).

[4] Choi S.U.S., Eastman J.A., "Enhancing Thermal Conductivity of Fluids with Nanoparticles", Argonne National Lab., IL (United States) (1995).

[5] Jani H.K., Modi K. V, A Review on Numerous Means of Enhancing Heat Transfer Rate in Solar- Thermal Based Desalination Devices, *Renew. Sustain. Energy Rev.*, **93**: 302–317 (2018).

[6] Falsafi M., Kargarsharifabad H., Numerical Study of Ferrofluid Forced Convection Heat Transfer in Tube with Magnetic Field, *Iut- Jcme*, **34(1)**: 11–25 (2015).

[7] Sheikholeslami M., Gorji-Bandpy M., Free Convection of Ferro Fluid in a Cavity Heated from below in the Presence of an External Magnetic Field, *Powder Technol.*, **256**: 490–498 (2014).

[8] Jafari A., Shahmohammadi A., Mousavi S. CFD Investigation of Gravitational Sedimentation Effect on Heat Transfer of a Nano-Ferrofluid, *Iran. J. Chem. Chem. Eng. (IJCCE)*, **34(1)**: 87-96 (2015)

[9] Habibi M., Amini M., Arefmanesh A., Ghasemikafrudi E., Effects of Viscosity Variations on Buoyancy-Driven Flow from a Horizontal Circular Cylinder Immersed in Al2O3-Water Nanofluid, *Iran. J. Chem. Chem. Eng. (IJCCE)*, **38(1)**:213-232 (2019).

[10] Goodarzi M, Safaei MR, Vafai K, Ahmadi G, Dahari M, Kazi SN, Jomhari N., Investigation of Nanofluid Mixed Convection in a Shallow Cavity Using a Two-Phase Mixture Model, *Int. J. Therm. Sci.*, **75:**204-220 (2014)**.**

[11] Yousefzadeh, S., Rajabi, H., Ghajari, N., Sarafraz M.M., Akbari O.A., Goodarzi M., Numerical Investigation of Mixed Convection Heat Transfer Behavior of Nanofluid in a Cavity with Different Heat Transfer Areas, *J. Therm. Anal. Calorim.*, **140**: 2779–2803 (2020)**.**

[12] Armaghani T., Ismael M.A., Chamkha A.J., Analysis of Entropy Generation and Natural Convection in an Inclined Partially Porous Layered Cavity Filled with a Nanofluid, *Can. J. Phys.*, **95(3)**: 238–252 (2017).

[13] Kargarsharifabad H., Experimental and Numerical Study of Natural Convection of Cu-Water Nanofluid in a Cubic Enclosure under Constant and Alternating Magnetic Fields, *Int. Commun. Heat Mass Transf.*, **119**: 104957 (2020).

[14] Sundar L.S., Singh M.K., Sousa A.C.M., Enhanced Heat Transfer and Friction Factor of MWCNT-Fe_3O_4/Water Hybrid Nanofluids, *Int. Commun. Heat Mass Transf.*, **52**: 73–83 (2014).

[15] Suresh S., Venkitaraj K.P.P., Selvakumar P., Chandrasekar M., Effect of Al_2O_3–Cu/Water Hybrid Nanofluid in Heat Transfer, *Exp. Therm. Fluid Sci.*, **38**: 54–60 (2012).

[16] Ranga Babu J.A., Kumar K.K., Srinivasa Rao S., State-of-Art Review on Hybrid Nanofluids, *Renew. Sustain. Energy Rev.*, **77**: 551–565 (2017).

[17] Kumar V., Sarkar J., Experimental Hydrothermal behavior of Hybrid Nanofluid for Various Particle Ratios and Comparison with other Fluids in Minichannel Heat Sink, *Int. Commun. Heat Mass Transf.*, **110**: 104397 (2020).

[18] Suresh S., Venkitaraj K.P., Selvakumar P., Chandrasekar M., Synthesis of Al_2O_3-Cu/Water Hybrid Nanofluids Using Two-Step Method and Its Thermo Physical Properties, *Colloids Surfaces A Physicochem. Eng. Asp.*, **388(1–3)**: 41–48 (2011).

[19] Selvakumar P., Suresh S., Use of Al_2O_3–Cu/Water Hybrid Nanofluid in an Electronic Heat Sink, *IEEE Trans. Compon., Packag., Manuf. Technol.*, **2(10)**: 1600–1607 (2012).

[20] Shahsavar A., Saghafian M., Salimpour M.R., Shafii M.B., Experimental Investigation on Laminar Forced Convective Heat Transfer of Ferrofluid Loaded with Carbon Nanotubes under Constant and Alternating Magnetic Fields, *Exp. Therm. Fluid Sci.*, **76**: 1–11 (2016).

[21] HAN W.S., Rhi S.H., Thermal Characteristics of Grooved Heat Pipe with Hybrid Nanofluids, *Therm. Sci.*, **15(1)**: 195–206 (2011).

[22] Sundar L.S., Singh M.K., Sousa A.C.M., Enhanced Heat Transfer and Friction Factor of MWCNT-Fe_3O_4/Water Hybrid Nanofluids, *Int. Commun. Heat Mass Transf.*, **52**: 73–83 (2014).

[23] Sarkar J., Ghosh P., Adil A., A Review on Hybrid Nano Fluids : Recent Research, Development and Applications, *Renew. Sustain. Energy Rev.*, **43**: 164–177 (2015).

[24] Mehryan S.A.M., Izadpanahi E., Ghalambaz M., Chamkha A.J., Mixed Convection Flow Caused by an Oscillating Cylinder in a Square Cavity Filled with Cu–Al_2O_3/Water Hybrid Nanofluid, *J. Therm. Anal. Calorim.*, **137(3)**: 965–982 (2019).

[25] Ismael M.A., Armaghani T., Chamkha A.J., Mixed Convection and Entropy Generation in a Lid-Driven Cavity Filled with a Hybrid Nanofluid and Heated by a Triangular Solid, *Heat Transf. Res.*, **49(17)**: 1645–1665 (2018).

[26] Zhou P., Zhong Y., Wang H., Fan L., Dong L., Li F., Long Q., Zheng T., Behavior of Fe/Nano-Si Particles Composite Electrodeposition with a Vertical Electrode System in a Static Parallel Magnetic Field, *Electrochim. Acta.*, **111**: 126–135 (2013).

[27] Mehryan S.A.M., Kashkooli F.M., Ghalambaz M., Chamkha A.J., Free Convection of Hybrid Al_2O_3-Cu Water Nanofluid in a Differentially Heated Porous Cavity, *Adv. Powder Technol.*, **28(9)**: 2295–2305 (2017).

[28] Nield D.A., Bejan A., Convection in Porous Media, Springer (2006).

[29] Kaviany M., Principles of Heat Transfer in Porous Media, Springer Science & Business Media (2012).

[30] Siavashi M., Yousofvand R., Rezanejad S., Nanofluid and Porous Fins Effect on Natural Convection and Entropy Generation of Flow Inside a Cavity, *Adv. Powder Technol.*, **29(1)**: 142–156 (2018).

[31] Leong J.C., Lai F.C., Mixed Convection in a Rotating Concentric Annulus with a Porous Sleeve, *J. Thermophys. Heat Transf.*, **33(2)**: 483–494 (2019).

[32] Das D., Roy M., Basak T., Studies on Natural Convection within Enclosures of Various (Non-Square) Shapes – A Review, *Int. J. Heat Mass Transf.*, **106**: 356–406 (2017).

[33] Muasavi S., Shahnazari M. Investigation of Natural Convection in a Vertical Cavity Filled with an Anisotropic Porous Media, *Iran. J. Chem. Chem. Eng. (IJCCE)*, **27(2)**:39-45 (2008).

[34] Tong T.W., Subramanian E., Natural Convection in Rectangular Enclosures Partially Filled with a Porous Medium, *Int. J. heat fluid flow.*, **7(1)**: 3–10 (1986).

[35] Mahdi R.A., Mohammed H.A., Munisamy K.M., Saeid N.H., Review of Convection Heat Transfer and Fluid Flow in Porous Media with Nanofluid, *Renew. Sustain. Energy Rev.*, **41**: 715–734 (2015).

[36] Kasaeian A., Azarian R.D., Mahian O., Kolsi L., Chamkha A.J., Wongwises S., Pop I., Nanofluid Flow and Heat Transfer in Porous Media: A Review of the Latest Developments, *Int. J. Heat Mass Transf.*, **107**: 778–791 (2017).

[37] Hatami M., Zhou J., Geng J., Song D., Jing D., Optimization of a Lid-Driven T-Shaped Porous Cavity to Improve the Nanofluids Mixed Convection Heat Transfer, *J. Mol. Liq.*, **231**: 620–631 (2017).

[38] Selimefendigil F., Ismael M.A., Chamkha A.J., Mixed Convection in Superposed Nanofluid and Porous Layers in Square Enclosure with Inner Rotating Cylinder, *Int. J. Mech. Sci.*, **124**–**125**: 95–108 (2017).

[39] Mehryan S.A.M., Izadi M., Namazian Z., Chamkha A.J., Natural Convection of Multi-Walled Carbon Nanotube–Fe_3O_4/Water Magnetic Hybrid Nanofluid Flowing in Porous Medium Considering the Impacts of Magnetic Field-Dependent Viscosity, *J. Therm. Anal. Calorim.*, **138(2)**: 1541–1555 (2019).

[40] Mohebbi R., Mehryan S.A.M., Izadi M., Mahian O., Natural Convection of Hybrid Nanofluids inside a Partitioned Porous Cavity for Application in Solar Power Plants, *J. Therm. Anal. Calorim.*, **137(5)**: 1719–1733 (2019).

[41] Karimdoost Yasuri A., Izadi M., Hatami H. Numerical Study of Natural Convection in a Square Enclosure Filled by Nanofluid with a Baffle in the Presence of Magnetic Field, *Iran. J. Chem. Chem. Eng. (IJCCE)*, **38(5)**: 209-220 (2019).

[42] Bahmani A., Kargarsharifabad H., New Integral Solutions for Magnetohydrodynamic Free Convection of Power-Law Fluids Over a Horizontal Plate, *Iran. J. Sci. Technol. - Trans. Mech. Eng.* **Online** (2020).

[43] Bahmani A., Kargarsharifabad H., Magnetohydrodynamic Free Convection of Non-Newtonian Power-Law Fluids over a Uniformly Heated Horizontal Plate, *Therm. Sci.*, **24(2B)**: 1323–1334 (2020).

[44] Eid M.R., Mabood F., Entropy Analysis of a Hydromagnetic Micropolar Dusty Carbon NTs-Kerosene Nanofluid with Heat Generation: Darcy–Forchheimer Scheme, *J. Therm. Anal. Calorim.* **Online:** 1–18 (2020).

[45] Gireesha B.J., Shankaralingappa B.M., Prasannakumar B.C., Nagaraja B., MHD Flow and Melting Heat Transfer of Dusty Casson Fluid over a Stretching Sheet with Cattaneo–Christov Heat Flux Model, *Int. J. Ambient Energy*. **Online:** 1–9 (2020).

[46] Hajatzadeh Pordanjani A., Aghakhani S., Karimipour A., Afrand M., Goodarzi M. Investigation of Free Convection Heat Transfer and Entropy Generation of Nanofluid Flow inside a Cavity Affected by Magnetic Field and Thermal Radiation, *J. Therm. Anal. Calorim.*, **137:** 997–1019 (2019)

[47] Mahmoudi A.H., Pop I., Shahi M., Talebi F., MHD Natural Convection and Entropy Generation in a Trapezoidal Enclosure Using Cu – Water Nanofluid, *Comput. FLUIDS*, **72**: 46–62 (2013).

[48] Mahmoudi A.H., Abu-Nada E., Combined Effect of Magnetic Field and Nanofluid Variable Properties on Heat Transfer Enhancement in Natural Convection, *Numer. Heat Transf. Part A Appl.*, **63(6)**: 452–472 (2013).

[49] Mejri I., Mahmoudi A., MHD Natural Convection in a Nanofluid-Filled Open Enclosure with a Sinusoidal Boundary Condition, *Chem. Eng. Res. Des.*, **98**: 1–16 (2015).

[50] Aminossadati S.M., Raisi a., Ghasemi B., Effects of Magnetic Field on Nanofluid Forced Convection in a Partially Heated Microchannel, *Int. J. Non. Linear. Mech.*, **46(10)**: 1373–1382 (2011).

[51] Rashad A.M., Armaghani T., Chamkha A.J., Mansour M.A., Entropy Generation and MHD Natural Convection of a Nanofluid in an Inclined Square Porous Cavity: Effects of a Heat Sink and Source Size and Location, *Chinese J. Phys.*, **56(1)**: 193–211 (2018).

[52] Ahmed S.E., Rashed Z.Z., MHD Natural Convection in a Heat Generating Porous Medium-Filled Wavy Enclosures Using Buongiorno's Nanofluid Model, *Case Stud. Therm. Eng.*, **14**: 100430 (2019).

[53] Sajjadi H., Delouei A.A., Izadi M., Mohebbi Rjij., Investigation of MHD Natural Convection in a Porous Media by Double MRT Lattice Boltzmann Method Utilizing MWCNT–Fe_3O_4/Water Hybrid Nanofluid, *Int. J. Heat Mass Transf.*, **132**: 1087–1104 (2019).

[54] Izadi M., Maleki N.M., Pop I., Mehryan S.A.M., Natural Convection of a Hybrid Nanofluid Subjected to Non-Uniform Magnetic Field within Porous Medium Including Circular Heater, *Int. J. Numer. Methods Heat Fluid Flow.*, **29(4)**: 1211–1231 (2019).

[55] Bejan A., A Study of Entropy Generation in Fundamental Convective Heat Transfer, *J. Heat Transfer.*, **101(4)**: 718 (1979).

[56] Bejan A., Second-Law Analysis in Heat Transfer and Thermal Design, *Adv. Heat Transfer.*, **15**: 1-58 (1982).

[57] Bejan A., "Entropy Generation Minimization: The Method of Thermodynamic Optimization of Finite-Size Systems and Finite-Time Processes", CRC Press, Boca Raton, New York. (1995).

[58] Yusuf T.A., Mabood F., Slip Effects and Entropy Generation on Inclined MHD Flow of Williamson Fluid through a Permeable Wall with Chemical Reaction via DTM, *Math Model. Eng Probl.*, **7(1)**: 1–9 (2020).

[59] Berrehal H., Mabood F., Makinde O.D., Entropy-Optimized Radiating Water/FCNTs Nanofluid Boundary-Layer Flow with Convective Condition, *Eur. Phys. J. Plus.*, **135(7)**: 535 (2020).

[60] Aghaei A., Sheikhzadeh G.A., Goodarzi M., Hasani H., Damirchi H., Afrand M., Effect of Horizontal and Vertical Elliptic Baffles inside an Enclosure on the Mixed Convection of a MWCNTs-Water Nanofluid and its Entropy Generation, *Eur. Phys. J. Plus*, **133**: 486 (2018).

[61] Goodarzi M, Safaei MR, Oztop HF, Karimipour A, Sadeghinezhad E, Dahari M, Kazi SN, Jomhari N. Numerical Study of Entropy Generation Due to Coupled Laminar and Turbulent Mixed Convection and Thermal Radiation in an Enclosure Filled with a Semitransparent Medium, *Sci. World J.*, **2014**: 761745 (2014).

[62] Ismael M.A., Armaghani T., Chamkha A.J., Conjugate Heat Transfer and Entropy Generation in a Cavity Filled with a Nanofluid-Saturated Porous Media and Heated by a Triangular Solid, *J. Taiwan Inst. Chem. Eng.*, **59**: 138–151 (2016).

[63] Al-Zamily A.M.J., Analysis of Natural Convection and Entropy Generation in a Cavity Filled with Multi-Layers of Porous Medium and Nanofluid with a Heat Generation, *Int. J. Heat Mass Transf.*, **106**: 1218–1231 (2017).

[64] Chamkha A.J., Rashad A.M., Mansour M.A., Armaghani T., Ghalambaz M., Effects of Heat Sink and Source and Entropy Generation on MHD Mixed Convection of a Cu-Water Nanofluid in a Lid-Driven Square Porous Enclosure with Partial Slip, *Phys. Fluids.*, **29(5)**: 52001 (2017).

[65] Chamkha A.J., Rashad A.M., Armaghani T., Mansour M.A., Effects of Partial Slip on Entropy Generation and MHD Combined Convection in a Lid-Driven Porous Enclosure Saturated with a Cu–Water Nanofluid, *J. Therm. Anal. Calorim.*, **132(2)**: 1291–1306 (2018).

[66] Mansour M.A., Ahmed S.E., Chamkha A.J., Entropy Generation Optimization for MHD Natural Convection of a Nanofluid in Porous Media-Filled Enclosure with Active Parts and Viscous Dissipation, *Int. J. Numer. Methods Heat Fluid Flow.*, **27(2)**: 379–399 (2017).

[67] Rashad A.M., Armaghani T., Chamkha A.J., Mansour M.A., Entropy Generation and MHD Natural Convection of a Nanofluid in an Inclined Square Porous Cavity: Effects of a Heat Sink and Source Size and Location, *Chinese J. Phys.*, **56(1)**: 193–211 (2018).

[68] Sheikholeslami M., Hatami M., Ganji D.D., Numerical Investigation of Nanofluid Spraying on an Inclined Rotating Disk for Cooling Process, *J. Mol. Liq.*, **211**: 577–583 (2015).

[69] Chamkha A.J., Mansour M.A., Rashad A.M., Kargarsharifabad H., Armaghani T., Magnetohydrodynamic Mixed Convection and Entropy Analysis of Nanofluid in Gamma-Shaped Porous Cavity, *J. Thermophys. Heat Transf.*, **34(4)**: 836–847 (2020).

[70] Prasad V., Kulacki F.A., Keyhani M., Natural Convection in Porous Media, *J. Fluid Mech.*, **150**: 89–119 (1985).

[71] Mahmud S., Fraser R.A., Magnetohydrodynamic Free Convection and Entropy Generation in a Square Porous Cavity, *Int. J. Heat Mass Transf.*, **47(14–16)**: 3245–3256 (2004).

[72] Ho C.J., Huang J.B., Tsai P.S., Yang Y.M., Preparation and Properties of Hybrid Water-Based Suspension of Al_2O_3 Nanoparticles and MEPCM Particles as Functional Forced Convection Fluid, *Int. Commun. Heat Mass Transf.*, **37(5)**: 490–494 (2010).

[73] Khanafer K., Vafai K., Lightstone M., Buoyancy-Driven Heat Transfer Enhancement in a Two-Dimensional Enclosure Utilizing Nanofluids, *Int. J. Heat Mass Transf.*, **46(19)**: 3639–3653 (2003).

[74] Maxwell J.C., "A Treatise on Electricity and Magnetism", Clarendon Press (1881).

[75] Sheikholeslami M., Bandpy M.G., Ellahi R., Zeeshan A., Simulation of MHD CuO–Water Nanofluid Flow and Convective Heat Transfer Considering Lorentz Forces, *J. Magn. Magn. Mater.*, **369**: 69–80 (2014).

[76] Takabi B., Shokouhmand H., Effects of Al_2O_3–Cu/Water Hybrid Nanofluid on Heat Transfer and Flow Characteristics in Turbulent Regime, *Int. J. Mod. Phys.*, **26(4)**: 1–25 (2015).

[77] Brinkman H.C., The Viscosity of Concentrated Suspensions and Solutions, *J. Chem. Phys.*, **20(4)**: 571 (1952).

[78] Pourmehran O., Rahimi-Gorji M., Hatami M., Sahebi S.A.R., Domairry G., Numerical Optimization of Microchannel Heat Sink (MCHS) Performance Cooled by KKL Based Nanofluids in Saturated Porous Medium, *J. Taiwan Inst. Chem. Eng.*, **55**: 49–68 (2015).

[79] Mabood F., Yusuf T.A., Khan W.A., Cu–Al_2O_3–H_2O Hybrid Nanofluid Flow with Melting Heat Transfer, Irreversibility Analysis and Nonlinear Thermal Radiation, *J. Therm. Anal. Calorim.*, (2020).

[80] Goodarzi M, Safaei MR, Karimipour A, Hooman K, Dahari M, Kazi SN, Sadeghinezhad E., Comparison of the Finite Volume and Lattice Boltzmann Methods for Solving Natural Convection Heat Transfer Problems Inside Cavities and Enclosures, *Abstr. Appl. Anal.*, **2014:** 762184 (2014)

[81] Goodarzi M, D'Orazio A, Keshavarzi A, Mousavi S, Karimipour A., Develop the Nano Scale Method of Lattice Boltzmann to Predict the Fluid Flow and Heat Transfer of Sir in the Inclined Lid Driven Cavity with a Large Heat Source Inside, Two Case Studies: Pure Natural Convection & Mixed Convection, *Phys. A.*, **509**: 210-233 (2018)

[82] Dogonchi A.S., Hatami M., Domairry G., Motion Analysis of a Spherical Solid Particle in Plane Couette Newtonian Fluid Flow, *Powder Technol.*, **274**: 186–192 (2015).

[83] Hatami M., Ganji D.D., Motion of a Spherical Particle on a Rotating Parabola Using Lagrangian and High Accuracy Multi-Step Differential Transformation Method, *Powder Technol.*, **258**: 94–98 (2014).

[84] Hatami M., Ganji D.D., Motion of a Spherical Particle in a Fluid Forced Vortex by DQM and DTM, *Particuology*, **16**: 206–212 (2014).

[85] Hatami M., Sheikholeslami M., Domairry G., High Accuracy Analysis for Motion of a Spherical Particle in Plane Couette Fluid Flow by Multi-Step Differential Transformation Method, *Powder Technol.*, **260**: 59–67 (2014).

[86] Mabood F., Pochai N., Optimal Homotopy Asymptotic Solution for Exothermic Reactions Model with Constant Heat Source in a Porous Medium, *Adv. Math. Phys.*, **2015** (2015).

[87] Bahmani A., Kargarsharifabad H., Laminar Natural Convection of Power-Law Fluids over a Horizontal Heated Flat Plate, *Heat Transf. Res.*, **48(3)**: 1044–1066 (2019).

[88] Aminossadati S.M., Ghasemi B., Natural Convection Cooling of a Localised Heat Source at the Bottom of a Nanofluid-Filled Enclosure, *Eur. J. Mech. B/Fluids.* **28(5)**: 630–640 (2009).

[89] M. Sheikholeslami M., Gorji Bandpy M., Ellahi R., Zeeshan A., Simulation of MHD CuO–Water Nanofluid Flow and Convective Heat Transfer Considering Lorentz Forces, *J. of Mag. Magnetic Material.*, **369**: 69-80 (2014).